Synthesis and Characterization of TiO2 Nanocrystals Prepared from n-Octadecylamine–Titanyl Oxalate Langmuir–Blodgett Films

ARTICLE *in* LANGMUIR · MARCH 2003

Impact Factor: 4.46 · DOI: 10.1021/la026720w

Synthesis and Characterization of TiO_2 Nanocrystals Prepared from *n*-Octadecylamine−Titanyl Oxalate Langmuir−Blodgett Films

A. Serra, A. Genga, D. Manno, G. Micocci, T. Siciliano, and A. Tepore

Dipartimento di Scienza dei Materiali, Università di Lecce ed Unità INFM, I-73100 Lecce, Italy

R. Tafuro and L. Valli*

Dipartimento di Ingegneria dell'Innovazione, Università di Lecce ed Unità INSTM, I-73100 Lecce, Italy

Received October 19, 2002. In Final Form: January 22, 2003

TiO_2 nanosized clusters have been prepared by the Langmuir−Blodgett technique starting from the *n*-octadecylamine−titanyl oxalate complex. The floating film morphology has also been investigated by Brewster angle microscopy (BAM). The presence of TiO_2 in the subphase promotes the formation of aggregates of *n*-octadecylamine on the subphase surface. LB films initially contain TiO_2 nanosized clusters embedded in the organic amorphous matrix; their structural evolution induced by thermal annealing has been investigated. UV−vis spectroscopy, high-resolution transmission electron microscopy (HRTEM), and small area electron diffraction (SAD) characterization methods are used as synergic techniques giving complementary information regarding both structural features and photophysical properties.

Introduction

Semiconducting nanosized clusters reveal dimension-dependent properties totally different from those of the corresponding polycrystalline materials.[1] Organized assemblies of crystallites show intriguing physical properties and form the subject of intense research in recent years.[2] The reduction of the particle size to nanoscale alters electrical, magnetic, electro-optical, and chemical properties. Therefore, the control of particle size represents an interesting opportunity to afford great flexibility to band-gap engineering in materials. This leads to applications such as nonlinear optical devices, fast switches, photovoltaic converters, and so on.[3−5]

Nanometer-sized semiconductor particles have been prepared by a wide range of synthetic methods, which involve homogeneous aqueous solutions,[6] glasses,[7] and surfactant systems such as vesicles, air−water monolayers, reversed micelles, and Langmuir−Blodgett films.[8−10]

According to the novel trend of assembling both nanometer scale structure and bulk materials using nanosized particles as building blocks, our approach uses the Langmuir−Blodgett technique for the deposition of layered organic−inorganic composite systems. Not only do Langmuir−Blodgett films offer the chance of built-in architectural control at the monolayer level, but they also provide useful media for the controlled construction of nanosized particles under very mild conditions.[11]

The aim of this paper is to analyze photophysical, structural, and morphological properties of TiO_2 nanosized clusters embedded in Langmuir−Blodgett films deposited from an *n*-octadecylamine−titanyl oxalate complex and also the film properties evolution after thermal annealing. UV−vis spectroscopy, high-resolution transmission electron microscopy (HRTEM), and small area electron diffraction (SAD) characterization methods are used as synergic techniques giving complementary information regarding both structural features and photophysical properties.

Experimental Section

Potassium titanyl oxalate, $K_2TiO(C_2O_4)_2$ (CARLOERBA analytical grade), and *n*-octadecylamine (Fluka, >99%) were used as received without further purification. The Langmuir−Blodgett films were deposited by a KSV5000 system 3 Langmuir−Blodgett apparatus (850 cm^2). *n*-Octadecylamine was dissolved in chloroform with a concentration of 4.9×10^{-4} M; the spreading solution was always used as soon as possible after preparation and stored in the dark in a refrigerator. In our depositions, 200 μL of the spreading solution was spread onto the subphase, whose temperature was regulated at 20 °C by a Haake GH D8 apparatus. The subphase was prepared by dissolving potassium titanyl oxalate (10^{-4} M solution) in ultrapure water (Millipore Milli-Q, resistivity 18.2 MΩ cm); the pH value was automatically buffered at 3.9.

After the solvent evaporated off, the floating film was compressed at a speed of 10 mm/min. The transfer on the substrates was performed at the surface pressure 30 mN/m and at the speeds 1 mm/min during the upstroke and 10 mm/min during the downstroke. The substrates were strongly hydrophilic quartz slides. They were washed for 3 h with ethyl acetate using

(1) Masumoto, Y.; Sonobe, K. *Phys. Rev. B* **1997**, *56*, 9734.
(2) Masumoto, Y. *J. Lumin.* **1996**, *70*, 386.
(3) Bawendi, M. G.; Steigerwald, M. L.; Brus, L. E. *Annu. Rev. Phys. Chem.* **1990**, *41*, 477.
(4) Brus, L. E. *J. Mater. Res.* **1989**, *4*, 704.
(5) Henglein, A. *Top. Curr. Chem.* **1988**, *143*, 113.
(6) H. Shin, H.; Collins, R. J.; De Guire, M. R.; Heuer, A. H.; Sukenik, C. N. *J. Mater. Res.* **1995**, *10*, 692.
(7) Borrelli, N. F.; Hall, D. W.; Holland, H. J.; Smith, D. W. *J. Appl. Phys.* **1987**, *61*, 5399.
(8) Stathatos, E.; Tsiorvas, D.; Lianos, P. *Colloids Surf., A: Physicochem. Eng. Aspects* **1999**, *149*, 49.
(9) Li, L. S.; Qu, L. H.; Lu, R.; Peng, X. G.; Zhao, Y. Y.; Li, T. J. *Thin Solid Films* **1998**, *329*, 408.
(10) Ohara, P. C.; Gelbart, W. M. *Langmuir* **1998**, *14*, 3418.
(11) Yang, J. H.; Chen, Y. M.; Bai, Y. B.; Xian, M.; Shen, D. F.; Wang, Y. Q.; Du, S. R.; Lu, R.; Li, T. J.; Wu, Y.; Xu, W. Q. *Supramol. Sci.* **1998**, *5*, 599.

10.1021/la026720w CCC: $25.00
Published on Web 03/04/2003

a Soxhlet extractor, dried in clean air, and placed in a mixture of 30% H_2O_2 and concentrated H_2SO_4 (1:3 by volume, respectively) for 15 min. Finally, they were rinsed well with ultrapure water and dried in clean air. Z-type deposition up to 80 layers was obtained onto hydrophilic quartz: the deposition ratio during lowering the substrate through the *n*-octadecylamine monolayer onto water was close to zero, while during withdrawing it was in the range 0.85−0.90.

The deposition ratio during the upstroke was scarcely affected by modifying deposition parameters such as surface pressure, dipping speed, and subphase temperature. This means that probably little material is picked up from the air−water interface while withdrawing the substrate.

Brewster angle microscopy (BAM) analysis was carried out using a NFT BAM2*Plus*−NIMA 601BAM apparatus. The instrument lateral resolution was 2 μm. Also in this case a compression speed of 10 Å^2 molecule^{-1} min^{-1} was utilized, after evaporation of chloroform spreading solvent.

All the deposited films were subsequently annealed in a cylindrical furnace at 150, 300, 400, 500, 600, and 800 °C in an oxygen flow of 200 sccm for 2 h. A heating and cooling rate of 1 °C/min was chosen to minimize thermal stress between the film and the substrate.

To perform transmission electron microscopy observations, both as-deposited and thermal annealed films were chemically removed from the substrates after exposure to hydrofluoric acid vapors and then deposited onto suitable grids. All observations were performed with a JEOL 2010 transmission electron microscope at 160 kV, representing the suitable acceleration voltage to obtain a sufficient resolution and minimal radiation damage of the material. High-resolution electron microscopy (HRTEM) and small area electron diffraction (SAD) results were obtained in order to investigate the morphology and structure of obtained thin films. SAD patterns were obtained by selecting a suitable spot size, convergence angle, and condenser aperture to get the diffraction patterns from chosen areas of about 100 nm in diameter with an approximately parallel beam (the convergence angle of the incoming beam was about 5×10^{-5} rad). HRTEM analysis has been performed in order to evidence the periodic structures in nanograins, to determine the size distribution of nanograins in the amorphous matrix. The particular features of the examined samples (nanocrystalline grains embedded in an amorphous matrix) give pictures characterized by a signal-to-noise ratio (S/N) that can be very low. In the present study we improved the S/N ratio through the convolution provided by a filter of circular apertures (Bragg filter) in the position of the maximum in the fast Fourier transform (FFT) of the experimental HRTEM images.

Spectrophotometric measurements were performed on both as-deposited and thermal annealed films in the wavelength range between 200 and 800 nm and recorded with a Varian Cary 5 UV−vis−NIR double-beam spectrophotometer at normal incidence with unpolarized light, equipped with an integrating sphere.

Results and Discussion

Langmuir Experiments. The isotherm of *n*-octadecylamine from chloroform spreading solution in the presence of potassium titanyl oxalate in the subphase at pH = 3.9 is illustrated in Figure 1 and is very similar to the one reported in the literature.[12]

The subphase pH has been explained by other researchers through the existence of titanium hydroxo colloids:[13]

$$[TiO(C_2O_4)_2]^{2-} + (n+1)H_2O = TiO_2{\cdot}nH_2O_{(colloid)} + 2C_2O_4^{2-} + 2H^+$$

The Langmuir isotherm discloses the formation of a monolayer which experiences "gaseous-like" phase (π = 0 mN/m) to "liquidlike" expanded phase (around π < 5 mN/m) to "solidlike" condensed phase (π > 10 mN/m) transitions and collapses at about 50 mN/m. The fully compressed floating film is remarkably rigid and sustained high surface pressures ($\pi \geq$ 40 mN/m). Such a floating film could be maintained at a pressure of 40 mN/m for several hours without significant area loss. It has been evidenced that solutions containing titanium ions are durable to construction of colloidal TiO_2 for no less than a month when refrigerated, principally for suspensions with low concentration of Ti(IV) and high concentration of H^+.[14] But, in our case, during all examinations the subphase was thermostated at 20 °C. Therefore, a freshly prepared subphase was always used during the Langmuir experiments; it was replaced every 2 days by a new subphase. The limiting area per molecule, $A_{\Pi\to 0}$, obtained by extrapolation of the steepest part of the curve at zero pressure, is about 32 Å^2. The rationale of the expansion of the limiting area with respect to the one reported in the literature in the case of pure water as the subphase[15] could be the interaction of the $-NH_3^+$ group with colloidal TiO_2 in the subphase. $A_{\Pi\to 0}$ could be greatly influenced by the dimension of TiO_2 nanoparticles instead of by the amino group cross section, thus confirming the observation that in acidic media the pattern of the Langmuir isotherm of stearylamine is dominated by the characteristics of the counterion.[16]

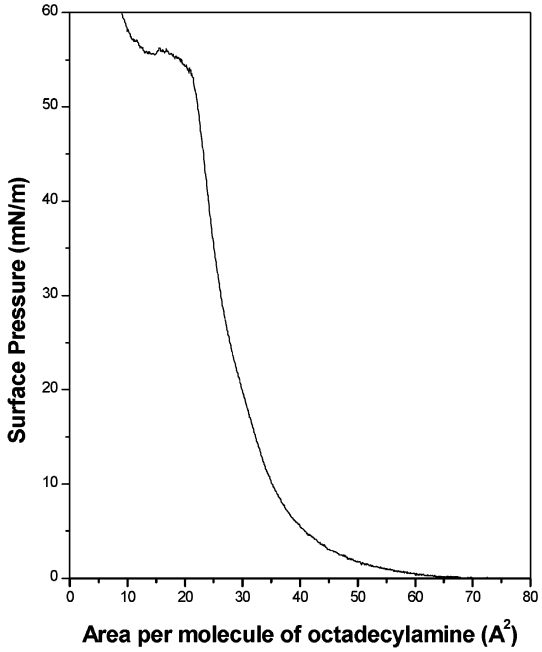

Figure 1. Pressure−area isotherm of *n*-octadecylamine in the presence of 10^{-4} M $K_2TiO(C_2O_4)_2$ in the aqueous subphase.

BAM investigations were made during the compression of the floating layer. The floating film appears profoundly affected by the presence of colloidal TiO_2 in the subphase. BAM observations have put in evidence an extremely different behavior depending on the presence or absence of TiO_2 nanoparticles. In fact, colloidal TiO_2 appears to promote association of stearylamine molecules locally in different regions of the water surface even at zero surface pressure after spreading solvent evaporation. The condensed/gas phase contemporaneous subsistence was dem-

(12) Ganguly, P.; Paranjape, D. V.; Sastry, M. *Langmuir* **1993**, *9*, 577.
(13) Van De Velde, G. M. H. *J. Inorg. Nucl. Chem.* **1977**, *39*, 1357.
(14) Comba, P.; Merbach, A. *Inorg. Chem.* **1987**, *26*, 1315.
(15) Mingotaud, A.-F.; Mingotaud, C.; Patterson, L. K. *Handbook of Monolayers*; Academic Press: San Diego, CA, 1993; p 390.
(16) Ganguly, P.; Paranjape, D. V.; Sastry, M. *J. Am. Chem. Soc.* **1993**, *115*, 793.

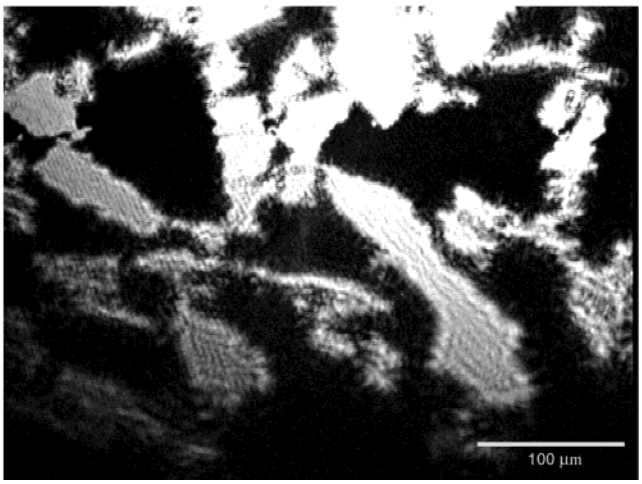

Figure 2. Morphology of an *n*-octadecylamine film on the water subphase containing 10^{-4} M $K_2TiO(C_2O_4)_2$ after spreading.

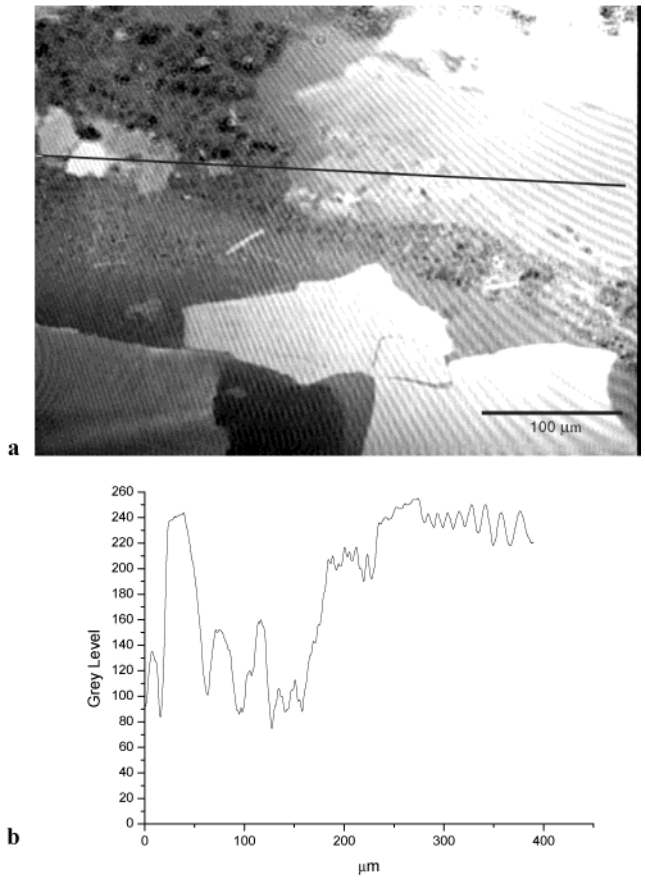

Figure 3. (a) Morphology of an *n*-octadecylamine film on the water subphase containing 10^{-4} M $K_2TiO(C_2O_4)_2$ at 5 mN/m. (b) Course of the reflectivity along the line drawn in picture a.

onstrated at low surface pressure and at low area density. It is possible to distinguish bright condensed phase islands and dark regions of gas phase. The large aggregates of octadecylamine onto the water subphase containing $K_2TiO(C_2O_4)_2$ are clearly apparent in Figure 2, and their average length is in the range 100−200 μm. In some cases, these wide domains are as large as the field of view of the BAM instrument (430 μm). During compression these domains coalesce and broaden. They begin to evidence more clearly facets and different shades of gray, as illustrated in Figure 3a. The variation in the floating film thickness and the presence of different phases are also

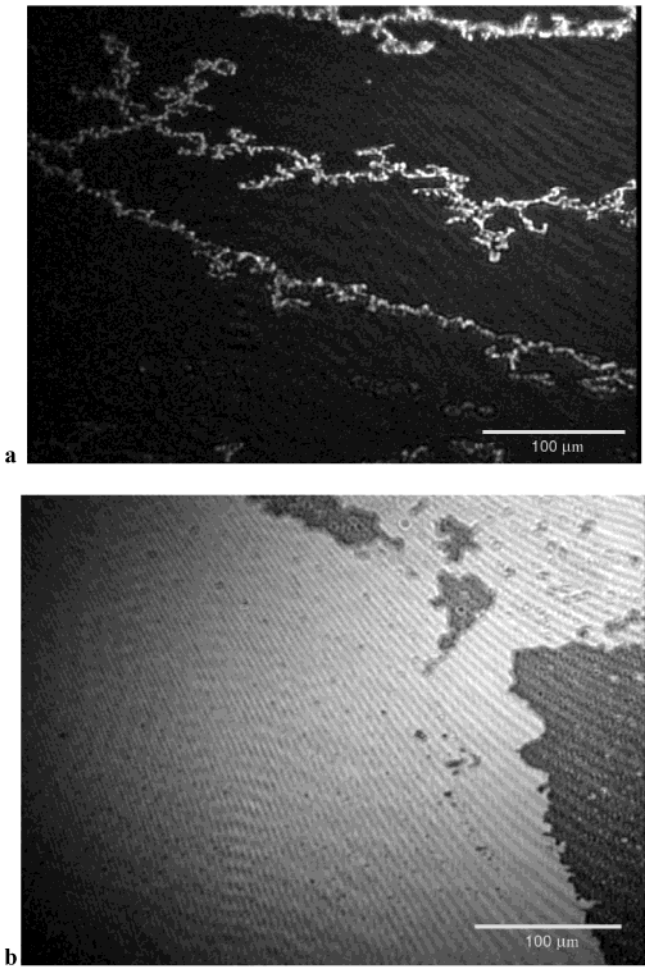

Figure 4. (a) Morphology of an *n*-octadecylamine film on the pure water subphase at 0 mN/m surface pressure. (b) Morphology of the same film at 10 mN/m.

confirmed by the course of reflectivity (Figure 3b) along a given line of the spread film (in Figure 3a). The highest gray levels correspond to the thicker aggregates of *n*-octadecylamine on the subphase surface, while the darkest small circular domains are consistent with the presence of deep holes in the floating film.

On the contrary, when pure water is used as the subphase, association at zero surface pressure is absolutely less pronounced (Figure 4a). A more uniform floating layer is obtained upon compression, as clearly evidenced by BAM micrograph at 10 mN/m, reported in Figure 4b. In conclusion, it is possible to state that BAM investigation manifests that *n*-octadecylamine bring us polycrystalline and condensed patches already as it is distributing on the subphase surface. TiO_2 provides rigidity to the floating layer and induces the substantial propensity to self-association and domain development.

The transfer of the floating layer onto strongly hydrophilic quartz and silicon supports was performed at 30 mN/m. The transfer ratios were 0.85−0.90 during the upstroke and close to zero during the downstroke, with the exception of the first two layers, for which the transfer ratios were both 1.1.

Concerning the kind of interactions that could be responsible for the film formation, in principle it is possible to hypothesize a competition between the protonated amine and TiO_2 in the electrostatic interaction with oxalate ions. In fact, most metal oxides are assumed to be covered with hydroxyl groups under normal conditions in water

solutions[17] and the TiO_2 surface is reported to be positively charged at pH ≤ 4.[18] But, in this connection, XPS data have revealed that it is not possible to claim such an ion-pairing mechanism as in the situation illustrated by Samha and DeArmond for stearic acid and ruthenium(II) complexes.[19] Also Sugai, using stearic acid and a Ti derivative, titanium bis(ammonium lactato),[20] did not observe such an ion-exchange reaction. On the contrary, Ganguly et al.[12] justified the use of *n*-octadecylamine during the deposition, as determined by the necessity of a cationic group in the surfactant in order to promote the transfer of the divalent anionic complex $[TiO(C_2O_4)_2]^{2-}$. Although it is reported that in the pH range 2-4 this divalent anionic species is stable,[21] in our films we have no evidence of the presence of the complex $[TiO(C_2O_4)_2]^{2-}$ (as demonstrated by XPS data).[22] Additionally, what makes the subject even more complex is that titanium aqueous solution chemistry is characterized by the development of several complexes and by sensitivity to processing parameters such as pH, temperature, concentration, and kind of anion. For example, Van De Velde in his studies on oxalate complexes of Ti(IV) in solution asserts that for pH above 3.0 it is possible to have $Ti(OH)_4$ precipitation.[23] Furthermore, the distribution diagram proposed by Van de Velde in the case of $(NH_4)_2TiO(C_2O_4)_2$ evidences that at pH = 3.9 the species in solution are $[Ti(OH)_2(C_2O_4)_2]^{2-}$ (about 80%) and $Ti(OH)_4$ (for the remaining 20%).

Etching of the quartz and silicon substrates by piranha solution (70:30 by volume, concentrated H_2SO_4/H_2O_2 proportion) was required in order to have strongly hydrophilic surfaces to obtain transfer ratios in the range 0.85−0.90 during the upstroke. The use of hydrophobized (by exposure to hexamethyldisilazane vapors) and not etched hydrophilic supports resulted in poor transfer ratios for both dipping directions. Probably, the formation process of films is governed by relatively weak hydrophobic and hydrophilic interactions. The weak hydrophobic−hydrophobic and hydrophilic−hydrophilic interactions will control the construction processes of the layers transferred onto the hydrophobic and hydrophilic quartz surfaces, respectively. The high surface coverage on the hydrophilic quartz surface is probably due to the stronger interaction for the hydrophilic−hydrophilic interface rather than the hydrophobic−hydrophobic interface. Silicon substrates etched by piranha solution have been used for TiO_2 film formation also by Kumar et al.[24]

The investigation aimed at clearing up and proposing a mechanism accounting for the film formation is also supported by other experimental data reported in the literature. Titanyl oxygens exhibit a larger basicity with respect to other metals [for example, V(IV)];[13] it is also specified that the second protonation of titanyl is easier than the first one, and the rationale is that the stability loss induced by protonation of the yl bond is more influential than the charge effect. It has been already observed that lysine and glutammic acid adsorb on the colloidal TiO_2 surface even with the occurrence of physically powerful electrostatic repulsion.[25,26] In this case the formation of hydrogen bonding has been advocated between the protonated amino group of stearylamine and TiO_2 surface hydroxyl groups. The $-NH_3^+$ group loses a proton as a consequence of adsorption in order to establish the interaction with the particle surface. This assumption is also supported by the very small value of adsorption enthalpy for lysine on the TiO_2 surface.[27] Such a transfer process appears to get along well with our experimental data. Additionally, the TEM analysis has revealed the presence in the as-deposited films of TiO_2 in the form of anatase and, according to Primet et al.,[28] the hydroxylic hydrogen atom is more proton-like in anatase than in rutile, thus assisting a mechanism developing through the proposed path.

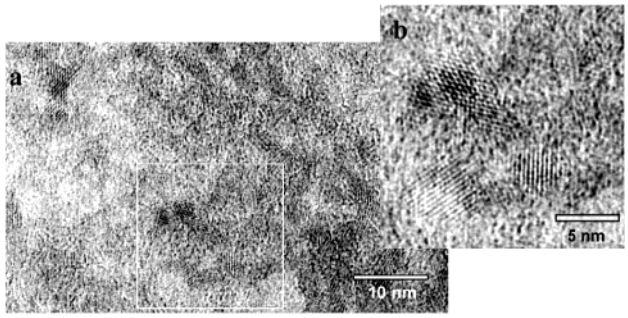

Figure 5. HRTEM image (picture a) recorded for the as-deposited, 30 monolayer LB film, together with the filtered image of the highlighted region (picture b).

The nature of interactions regulating the film transfer from the subphase has been indirectly suggested also by the result obtained when arachidic acid was used instead of stearylamine. In fact, in principle, it is also possible to suppose that colloidal TiO_2 could remain "mechanically" trapped within the long tails of arachidic acid molecules. But, in such experiments, according to Sugai's investigations, we did not observe the transfer of TiO_2 nanoparticles from the subphase. Thus, such "mechanical transfer" could not be proposed in order to explain the presence of TiO_2 in the film.

Similar deposition attempts for the transfer of TiO_2 on the substrates were also carried out at pH = 1 for the subphase, obtained through controlled additions of diluted HCl. But under these circumstances no presence of colloidal TiO_2 onto the substrate has been detected, according to the distribution diagram proposed in ref 23 in the case of $(NH_4)_2TiO(C_2O_4)_2$. At this pH value, the $Ti(OH)_4$ concentration is practically negligible, while $[Ti(OH)_2(C_2O_4)_2]^{2-}$ and $Ti(OH)_2(H_2O)_2(C_2O_4)_2$ are the prevalent species.

Morphological and Structural Analysis. Figure 5 shows a typical HRTEM image (picture a) recorded from the as-deposited, 30 layer thick LB film, together with the filtered image of the highlighted region (picture b). As apparent, the thin film consists of a short-range order matrix where a lot of nanocrystals are dispersed. Figure 6 illustrates a typical HRTEM image (picture a) recorded from the 500 °C thermal annealed, 30 layer thick LB film, together with the filtered image of the highlighted region (picture b). It is apparent that the nanocrystals, dispersed

(17) Boehm, H. P. *Discuss. Faraday Soc.* **1971**, *52*, 264.
(18) Kalyanasundaran, K.; Vlachopoulos, N.; Krishnan, V.; Monnier, A.; Gräzel, M. *J. Phys. Chem.* **1987**, *91*, 2342.
(19) Samha, H.; DeArmond, M. K. *Langmuir* **1994**, *10*, 4157.
(20) Sugai, H.; Hoshi, N.; Iijima, T.; Masumoto, H. *Jpn. J. Appl. Phys.* **1998**, *37*, 5118.
(21) Potdar, H. S.; Deshpande, S. B.; Date, S. K. *Mater. Chem. Phys.* **1999**, *58*, 121.
(22) Malitesta, C.; Tepore, A.; Valli, L.; Genga, A.; Siciliano, T. *Thin Solid Films* **2002**, *422*, 112−119.
(23) Van De Velde, G. M. H. *J. Inorg. Nucl. Chem.* **1977**, *39*, 1357.
(24) Kumar, P. M.; Badrinarayanan, S.; Sastry, M. *Thin Solid Films* **2000**, *358*, 122.
(25) Giacomelli, C. E.; Avena, M. J.; De Pauli, C. P. *Lanmguir* **1995**, *11*, 3483.
(26) Tentorio, A.; Canova, L. *Colloids Surf.* **1989** *39*, 311.
(27) Okasaki, S.; Aoki, T.; Tani, K. *Bull. Chem. Soc. Jpn.* **1981**, *54*, 1595.
(28) Primet, M.; Pichat, P.; Mathieu, M. V. *J. Phys. Chem.* **1971**, *75*, 1216 and 1221.

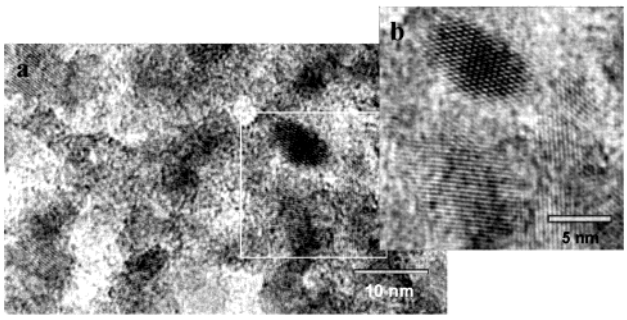

Figure 6. HRTEM image (picture a) recorded for the thermal annealed, 30 monolayer LB film (at 500 °C), together with the filtered image of the highlighted region (picture b).

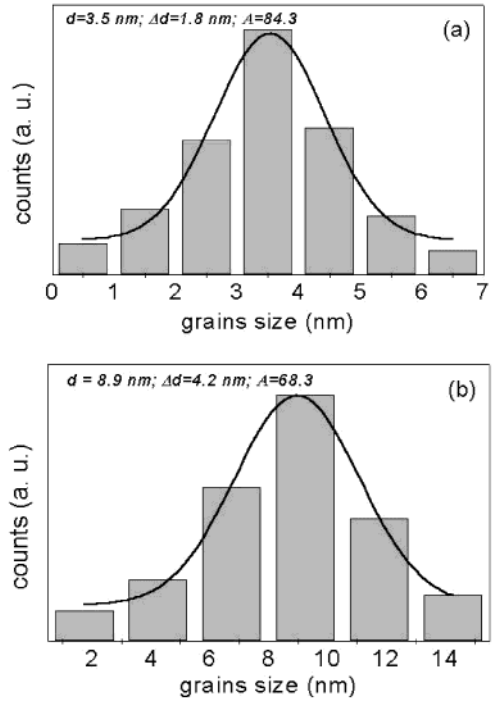

Figure 7. Histograms for the as-deposited (picture a) and thermal annealed film at 500 °C (picture b).

in the amorphous matrix, are larger in diameter with respect to the as-deposited material.

The determination of the nanograin size distribution is obtained by a micrometer eyepiece with resolution better than 0.01 cm and was performed directly onto negative plates recorded at 400000×, thus allowing us to measure the grain diameters with a resolution better than 0.25 nm. Typical histograms for the as-deposited and thermal annealed films at 500 °C are depicted in parts a and b of Figure 7, respectively. In the as-deposited sample, the nanograin diameters are monodispersed and the distribution peak is around 3.5 nm, with a broad tail extending up to 7 nm. In the 500 °C annealed sample, the nanograin diameters are monodispersed and the distribution peaks arise around 8.9 nm, with a broad tail extending up to 14 nm. The histograms clearly reflect the convolution of the distributions of the nanocrystals constituting the different samples. To extract their individual size and radius dispersion, we performed a numerical deconvolution of the histogram. We assume the histograms to be composed of one nanocrystal species characterized by a Gaussian distribution of diameters of amplitude A and half-width Δd spread around the average diameter d. The Gaussians with the best-fit parameters A, Δd, and d are superimposed in the histograms of Figure 7. A summary of the d values

Table 1. d Values and Their Relative Dispersion (Δd) Obtained from Deconvolution of HRTEM Images Recorded on Different Annealed Films

sample	d (nm)	Δd (nm)
as-deposited	3.5	1.8
150 °C annealed	4.5	2.1
300 °C annealed	5.9	2.8
400 °C annealed	7.6	3.3
500 °C annealed	8.9	4.2
600 °C annealed	9.0	4.4
800 °C annealed	9.0	4.3

and of their relative dispersion (Δd), obtained from deconvolution of HRTEM images recorded on different annealed films, is reported in Table 1. It is apparent that the grain size increases continuously up to the temperature 500 °C; then, for higher annealing temperatures, it attains the constant value about 9 nm.

Figure 8 shows typical diffraction patterns coming from an as-deposited (picture a) and a thermal annealed film (at 500 °C, picture b). It is apparent that the diffraction rings, initially very broad in Figure 8a, are sharpened as a consequence of the thermal annealing (Figure 8b). The interplanar spacings determined from both the diffraction patterns are reported in Table 2 together with the corresponding ones of the TiO_2 anatase phase reported in the literature[29] for comparison. It is apparent that the crystalline agglomerates, visible in the amorphous matrix, are TiO_2 in the anatase phase for both as-deposited and thermal annealed materials. On the contrary, we can also conclude that the octadecylamine molecules give generation to the amorphous matrix in which such crystalline TiO_2 agglomerates are dispersed. The thermal annealing induces only an increase of structural order in TiO_2 grains.

Optical Properties. Figure 9 shows typical transmittance and reflectance spectra recorded on an as-deposited sample. The abrupt decrease in transmittance at low wavelength indicates the onset of interband absorption (fundamental absorption edge). By a numerical procedure based on the model of Heaven,[30] the optical constants of our films, refraction index, n, and extinction coefficient, k, were determined from transmission and reflection measurements at normal incidence. Then the absorption coefficient $\alpha = 4\pi k/\lambda$ was obtained. It is well-known that, near the fundamental absorption edge, the absorption coefficient can be written as[31]

$$\alpha h\nu = B(h\nu - E_g)^m \qquad (1)$$

where E_g is the optical band gap corresponding to the transition indicated by the value of m. The factor B depends on the transition probability and can be taken as constant within the investigated optical frequency range. Let $Y = \alpha h\nu$ and Y' be the first derivative of Y with respect to photon energy; from eq 1 one obtains:

$$Y/Y' = (h\nu - E_g)/m \qquad (2)$$

Y and Y' are determined from experimental data, and m and E_g represent the slope and the intercept of the linear plot Y/Y' versus $h\nu$.

Figure 10 shows the plot of Y/Y' as a function of photon energies for the as-deposited sample.

(29) Suhail, M. H.; Mohan Rao, G.; Mohan, S. *J. Appl. Phys.* **1992**, *71*, 1421.
(30) Heavens, O. S. In *Physics of Thin Films*; Hass, G., Thun, R. E., Eds.; Academic Press: New York, 1964.
(31) Burns, G. *Solid State Physics*; Academic Press: New York, 1985.

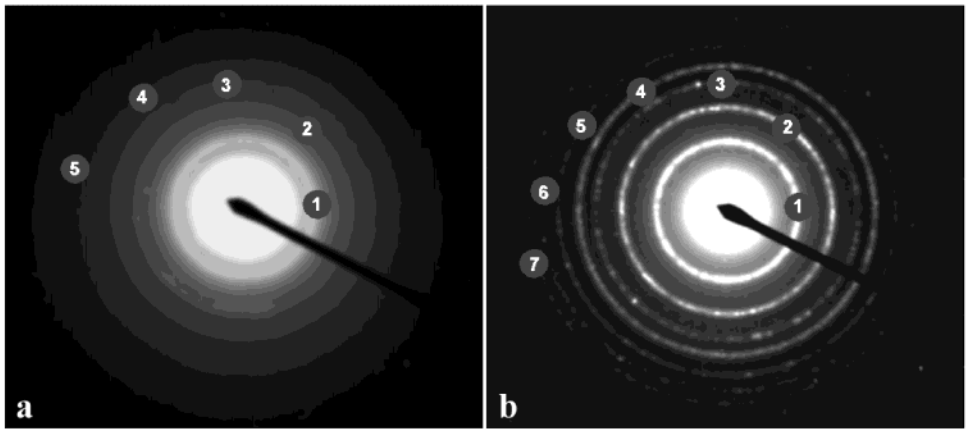

Figure 8. Diffraction patterns coming from as-deposited (picture a) and 500 °C thermal annealed films (picture b).

Table 2. Interplanar Spacings Deduced from the Electron Diffraction Patterns Reported in Figure 8 together with the Corresponding Ones Obtained from Literature Data[38] Regarding the Anatase Phase of Titanium Oxide[a]

interplanar spacings determined in this work		interplanar spacings reported in the lit.
(*n*) *d* (nm) as-deposited	(*n*) *d* (nm) 500 °C thermal annealed	*d* (nm)—*hkl*
(1) 0.351	(1) 0.352	0.3516—011
(2) 0.232	(2) 0.234	0.2332—112
(3) 0.188	(3) 0.187	0.1856—201
(4) 0.166	(4) 0.165	0.1666—121
(5) 0.146	(5) 0.145	0.1493—213
	(6) 0.136	0.1379—124
	(7) 0.124	0.1233—223

Numbers in parentheses (*n*) represent the labels of reflections in diffraction patterns, and *hkl* represents the related Miller index.

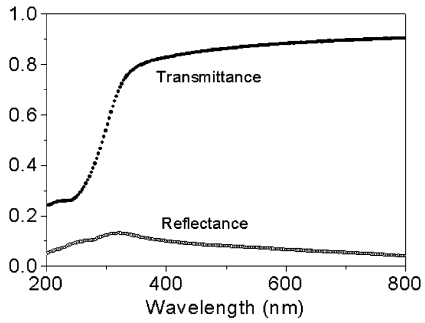

Figure 9. Transmittance and reflectance spectra recorded on an as-deposited sample.

There are clear-cut linear regions corresponding to allowed indirect transitions with an optical energy gap of about 3.60 eV. Likewise, the energy gaps of annealed samples have been determined and the obtained results are summarized in Table 3. It is apparent that an allowed indirect transition takes place; the related energy gap ranges between 3.46 and 3.60 eV and decreases with the annealing temperature. This effect is clearly demonstrated in Figure 11, which reports typical absorbance spectra obtained in the 200—800 nm range for as-deposited and two thermally annealed samples (at 500 and 800 °C). As can be inferred, the typical band due to TiO_2 progressively shifts to longer wavelengths and its absorbance at the band maximum (A_{max}) decreases. The absorption threshold of the as-deposited films is about 344 nm, 29 nm blue shifted from that of bulk anatase TiO_2[32] and 43 nm blue shifted from that of polycrystalline anatase TiO_2.[33] The blue shift decreases with thermal treatment. In fact, the films annealed at 500 °C show an absorption threshold of about 358 nm, 15 nm blue shifted with respect to that of bulk anatase TiO_2 and 28 nm blue shifted from that of polycrystalline anatase TiO_2. Further thermal treatments do not modify the optical properties: the 800 °C

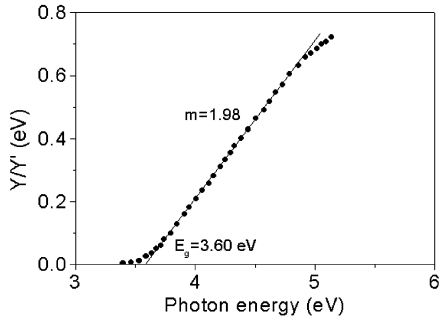

Figure 10. Plot of Y/Y' as a function of photon energies for the as-deposited sample.

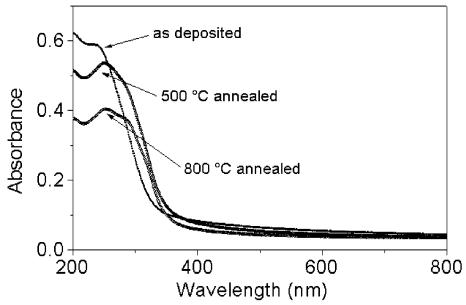

Figure 11. Absorbance spectra obtained in the range 200—800 nm for as-deposited, 500 and 800 °C thermal annealed samples.

Table 3. Energy Gaps Determined for All Analyzed Films

sample	energy gap (eV)
as-deposited	3.60
150 °C annealed	3.57
300 °C annealed	3.54
400 °C annealed	3.49
500 °C annealed	3.46
600 °C annealed	3.46
800 °C annealed	3.46

(32) Choi, W.; Termin, A.; Hoffmann, M. R. *J. Phys. Chem.* **1994**, *98*, 13671.
(33) Tang, H.; Prasad, K.; Schmid, P. E.; Levy, F. *J. Appl. Phys.* **1994**, *75*, 2042.

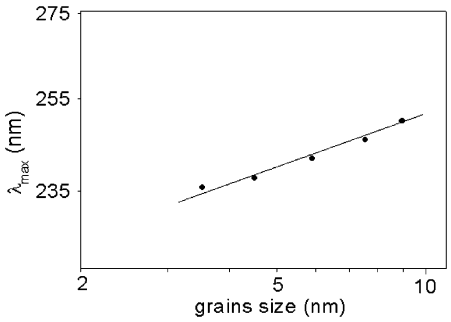

Figure 12. Experimental values of the wavelength at the band maximum (λ_{max}) of TiO_2 nanoparticles as a function of the nanoparticle diameter (d).

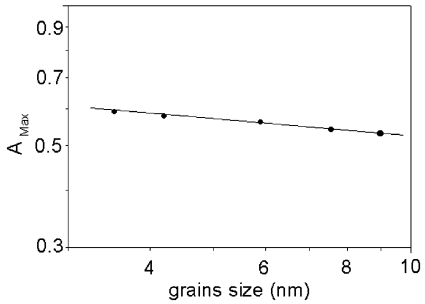

Figure 13. A_{max} as a function of nanoparticle diameter (d).

annealed films show only a contraction in the absorbance intensity. This observation indicates that probably below 500 °C the process of TiO_2 crystalline aggregation is dominant; on the contrary, over 500 °C, the disaggregation of TiO_2 nanograins compensates such crystalline aggregation. In addition, at higher temperatures, partial evaporations of the last embedded octadecylamine molecules can occur.

The evident blue shift of our films comes from a quantum confinement effect caused by the small particle size. It is well-known that, as a consequence of quantum confinement of the electron−hole pair, the absorption spectrum of semiconductor nanoparticles is size dependent. This is shown in Figure 12, where the experimental values of the wavelength at the band maximum (λ_{max}) of TiO_2 nanoparticles are plotted as a function of the nanoparticle diameter (d).[34] We have found that these data can be approximately described by the following power law

$$\lambda_{max} = 214.4 d^{0.07} \tag{3}$$

From an analysis of the A_{max} as a function of d data (Figure 13) it results that

$$A_{max} \propto d^{-0.114} \tag{4}$$

Correlating the A_{max} value to the nanoparticle surface density (i.e. to the surface/volume ratio), the expected dependence should be $\propto d^{-1}$ for a geometrical sphere whereas for a fractal-like sphere it should be $\propto d^{\beta}$, with β ranging from 0 to −1.[35,36] As a consequence, eq 4 suggests that TiO_2 nanoparticles display surface irregularities according to TEM observations.

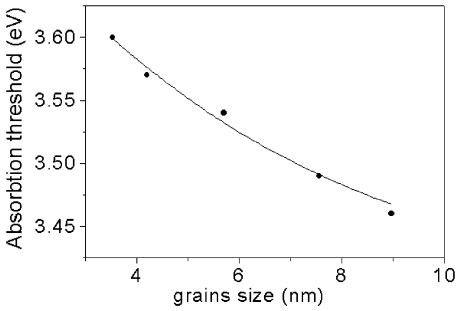

Figure 14. Absorption threshold values as a function of nanograins diameter.

The diameter of the TiO_2 nanocrystals and the absorption thresholds (A_p) can be also related by the semiempirical relationship:

$$A_p = A_b + \frac{C_1}{d^2/4} + \frac{C_2}{d/2} \tag{5}$$

proposed by Fendler[37] to overcome the uncertainties in the hole and electron effective mass values for size-quantized anatase TiO_2 particles. In eq 5 A_b is the absorption threshold of the bulk anatase TiO_2 semiconductor and C_1 and C_2 are constants. In Figure 14 we have plotted the absorption threshold as a function of nanograin diameter. The experimental data are perfectly fitted by eq 5 with the following values of parameters: $C_1 = 0.19$ nm^2 eV and $C_2 = 0.01$ nm eV.

Conclusions

TiO_2 nanosized clusters were embedded in Langmuir−Blodgett films prepared from an *n*-octadecylamine−titanyl oxalate complex. The introduction in the water subphase of $K_2TiO(C_2O_4)_2$ promotes the generation of large aggregates in the floating films even at very low surface pressure values. BAM investigations evidence the presence of regions with very different reflectivity. The structural evolution of LB films induced by thermal annealing has been investigated. UV−vis spectroscopy, high-resolution transmission electron microscopy (HRTEM), and small area electron diffraction (SAD) characterization methods are used as synergic techniques giving complementary information regarding both structural features and photophysical properties.

The crystalline structure of nanosized TiO_2 was anatase for both as-deposited and thermal annealed materials. The thermal treatment causes only an increase of structural order: in fact, as confirmed by HRTEM observations, the mean nanocrystal size increases as the annealing temperature increases too.

The photophysical properties of our films closely depend on nanocrystal size, and the optical absorption characteristics come from quantum confinement of the electron−hole pair in titanium oxide nanoparticles.

LA026720W

(34) Nakaoka, Y.; Nosaka, Y. *Langmuir* **1997**, *13*, 708.
(35) Pfeifer, P.; Avnir, D. *J. Chem. Phys.* **1983**, *79*, 3558.
(36) Avnir, D.; Farin, D.; Pfeifer, P. *J. Chem. Phys.* **1983**, *79*, 3566.
(37) Fendler, J. H. *Membrane-Mimetic Approach to Advanced Materials*; Springer-Verlag: Berlin, 1994.
(38) Suhail, M. H.; Mohan, R. G.; Mohan, S. *J. Appl. Phys.* **1992**, *71*, 1421.